Progress In Electromagnetics Research Letters, Vol. 48, 7–13, 2014

Tailoring the Properties of Photonic Nanojets by Changing the Material and Geometry of the Concentrator

Abdul Khaleque* **and Ziyuan Li**

Abstract—Some microobjects can concentrate an incoming incident plane wave and produce the so-called photonic nanojets. The highly focused emerging beams have a high intensity and can be used in applications in microscopy, beam manipulation and imaging. In this article, it is shown that an adequate choice of geometric shape and material can lead to an improvement of the electric field enhancement capacity of nanojets by a factor of 40%.

1. INTRODUCTION

Lasers have different sizes and shapes: from bulk lasers to tiny integrated nano-lasers, these devices have revolutionized the way we handle information, materials and physical and chemical variables. In order to produce very tiny lasers, different techniques have been used in the past, such as total internal reflection in high refractive index contrast structures [1–4], photonic bandgap effect [5–9] and the excitation of plasmonic waves [10–13]. In general, high refractive index contrast lasers emit power in the range of microwatts to a few milliwatts, while photonic crystal lasers emit power in the range of picowatts to microwatts (in general, photonic crystal band-edge [7] and surface emitting lasers [9] emit significantly more power than single-defect lasers) and plasmonic lasers emit nanowatts optical power. If higher power is needed, bulk or fiber lasers [14, 15] needs to be used to drive optical devices.

On the other hand, although optical fiber passive devices [16–21] can handle higher power, they do not offer much flexibility and occupy a large physical volume. If additional functionalities need to be added to a system, a better approach is to process the laser signals by using integrated optical devices. However, free-space and optical fibers remain attractive to transport signals at very high speed over medium and long distances (e.g., from one computer board to another): thereby there is a necessity of coupling light in and out from integrated optical devices to optical fibers and/or free-space. In addition to optical communications and computer applications, light coming from a bulk laser needs to be focused into very small spots in high resolution microscopy and nano-patterning applications.

There are different ways to couple light from free-space/optical fiber into integrated circuits by using, for example, grating couplers [22] or micro-objects (micro-cylinders) to create the so-called photonic nanojets [23]. Nanojets are subwavelength tightly focused electromagnetic beams that emerge from a micro-object when it is illuminated by a plane wave — the so-called nanojets have been observed at optical [24] and microwave [25] frequencies. At optical frequencies, the spot-size diameters of nanojets range between 200 and 500 nm [26, 27] and are the result of multiple scattering [28] in the micro-object. The position and polarization of the incident beam can control the position and size of photonic nanojets [29]. Besides applications in coupling light into integrated optical circuits and microscopy, nanojets could be used in two-photon fluorescence enhancement, maskless nano-patterning, detection of nano-particles, optical trapping and data storage. Another potential application of nanojets is the enhancement of Raman scattering [30] with enhancement factors in the order of 10000, being potentially

Received 21 May 2014, Accepted 29 July 2014, Scheduled 8 August 2014

* Corresponding author: Abdul Khaleque (abdul.khaleque@student.adfa.edu.au).

The authors are with the School of Engineering and Information Technology, University of New South Wales at Canberra, ACT 2610, Australia.

used to any material. However, it should be mentioned that plasmonic devices can lead to enhancement of Raman scattering by factors above 1 million [31–34].

In a recent paper, Ju and coworkers [35] have placed a metal below a microcylinder and excited surface plasmon polaritons from a plane wave. The addition of the metal improved the electric field enhancement factor of the structure and, by physically changing the thickness of the microdisk, some of the properties of the nanojet could be controlled. In this article, we study how different geometric micro-objects affect plasmonic nanojets: it is shown that certain shapes (e.g., linear shape) can lead to higher electric field enhancement in plasmonic nanojets. We also show that the choice of metal underneath the microobject strongly influences the electric field enhancement factor.

2. CYLINDRICAL, HYBRID LINEAR AND HYBRID PARABOLIC DIELCTRIC CONCENTRATORS WITH DIFFERENT METALIC LAYERS BELOW THE COLLIMATOR

Figures 1(a)–(c) show the basic structures that will be analyzed in this article: a standard microdisk, a hybrid linear-microdisk shape and a hybrid microdisk-parabolic shape. The substrate and the dielectric concentrators (e.g., microcylinder or microdisk as shown in Figure 1(a)) are assumed to be made of quartz. A metallic layer of thickness of 100 nm is placed below the dielectric concentrators. In order to study the effects of different metals on nanojets, three common metals are chosen: gold, silver and aluminium. Starting from the basic micro-cylindrical structure, we change the reference cylindrical shape (Figure 1(a)) to a hybrid cylindrical-linear (Figure 1(b)) and a hybrid cylindrical-parabolic shape (Figure 1(c)). In order to simplify the notation, we call a hybrid semi-cylindrical/semi-linear and a semi-cylindrical/semi-parabolic just as hybrid linear and hybrid parabolic, respectively.

The incident wave is assumed to be a plane wave propagating along the $+x$ direction (coordinate system shown in Figures 1(a), 1(b) and 1(c)) and air is the surrounding the whole structure. Commercial three dimensional ($3D$) Finite Difference Time Domain (*FDTD)* software (*RSOFT FULLWAVE*) is used to analyze the basic properties of the structures [36]. The grid sizes of the metallic regions are chosen as $\Delta x = \Delta y = \Delta z = 5\,\text{nm}$, while the grid sizes in the dielectric layers are chosen as $\Delta x = \Delta y = \Delta z = 30\,\text{nm}$. The time step is chosen to be well below the stability limit to avoid divergence of the *FDTD* code: in our case, $\Delta t = 6.67 \times 10^{-18}\,\text{s}$. The computational area is terminated by Perfectly Matching Layers (*PML*) and the metallic region does not reach the *PML* to avoid computational instabilities in the *FDTD* code, although special PMLs could be constructed for metallic and dispersive materials [37]. In this simulation, the refractive index of quartz is chosen as 1.54 while metals are modeled as dispersive materials with relative electric permittivity described as [36],

$$\varepsilon_{metal}\left(\omega_{FW}\right) = 1 + \sum_{m=1}^{6} \frac{\Delta\varepsilon_m}{-a_m\omega_{FW}^2 - ib_m\omega_{FW} + c_m} \tag{1}$$

where a_m, b_m, c_m and $\Delta\varepsilon_m$ are coefficients that are built-in in software material library [36], and $\omega_{FW} = 2\pi/\lambda_0$ is the *Fullwave* computational frequency with λ_0 being the free-space wavelength in

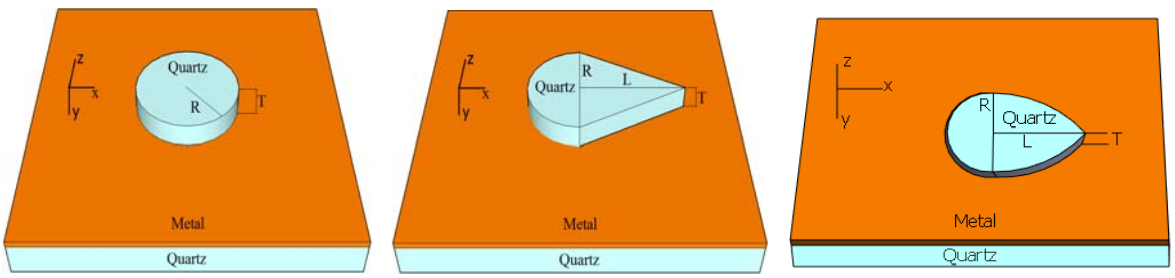

Figure 1. Schematic of dielectric concentrators: (a) cylindrical, (b) hybrid linear, and (c) hybrid parabolic.

units of μm. The values of the coefficients can be found in the *RSOFT Fullwave manual* [36]. Since the metallic layer covers a significant area in the x-y plane, the incident electric field is assumed to be polarized along the vertical direction (E_y) while the incident plane wave is propagating along the $+x$ direction, allowing the excitation of plasmonic waves [38]. Electric field monitors are placed close to the source and at the 'end' of the structures to assess the electric field enhancement factor.

The electric field enhancement factor is calculated as,

$$F_{enh} = \frac{E_{tip}}{E_{inc}} \tag{2}$$

where E_{inc} is the magnitude of the incident electric field of the plane wave and E_{tip} is the magnitude of the electric field at the 'end' of the concentrator (where it reaches a maximum value) and close to the metallic surface.

3. RESULTS AND DISCUSSIONS

The structures are designed to work at the free-space wavelength (λ) of 850 nm. An initial reference microdisk concentrator on top of a gold sheet is optimized to work at 850 nm, as shown in Figure 1(a). The optimized parameters are $R = 3.05$ μm, $T = 1.0$ μm. The electric field enhancement factor is about 4.95 (intensity enhancement of about 24.5). It should be mentioned that some software packages such as *RSOFT Fullwave* [36] provide readings of the square of the electric field ($|E|^2$) instead of the magnitude of the electric field which can lead to erroneous interpretation of results. Next, the front semi-circle is changed to linear (as shown in Figure 1(b)) and parabolic shapes (as shown in Figure 1(c)) with length $L \geq R$ (smaller values of L lead to lower values of F_{enh}). There is no significant improvement of F_{enh} by changing the length (L) (as shown in Figure 3) and thickness (T). In addition to that, the effect of three different metals (gold, silver and aluminium) is also analyzed, with main results summarized in Table 1.

Table 1. Maximum electric field enhancement factors for different structures and metals.

Geometrical shape	Material	Maximum value of F_{enh}
Cylindrical	Gold	4.95
	Silver	5.60
	Aluminium	2.20
Hybrid Linear	Gold	5.20
	Silver	6.20
	Aluminium	1.74
Hybrid Parabolic	Gold	4.49
	Silver	5.43
	Aluminium	2.20

The effects of the geometrical shape on F_{enh} are examined for a gold film: it is clear that a hybrid linear structure gives the highest electric field enhancement when compared with the cylindrical or hybrid parabolic shapes. Although in some applications (e.g., coupling to waveguide [7]), parabolic tapers provide better tapering of the incident wave into a smaller area, the round shape at the end of the taper (as seen in Figure 2(c)) may lead to a larger spot-size diameter at the exit of the micro-object and, consequently, to a lower electric field enhancement as shown in Table 1. On the other hand, the hybrid linear concentrator can better localize the incident light at the end of the linear taper (lightning rod effect) as can be observed in Figure 2(a) but the localized light quickly diverges as it propagates along the surface of the metal. As reference, the electric field profile of a cylindrical structure is shown in Figure 2(b) — it can be seen that light emerging from the cylinder remains collimated over some distance. A similar conclusion can be drawn for the hybrid parabolic concentrator. The hybrid linear shape provides an improvement in F_{enh} ranging from 5% to 11% (or 11% to 23% increase in intensity)

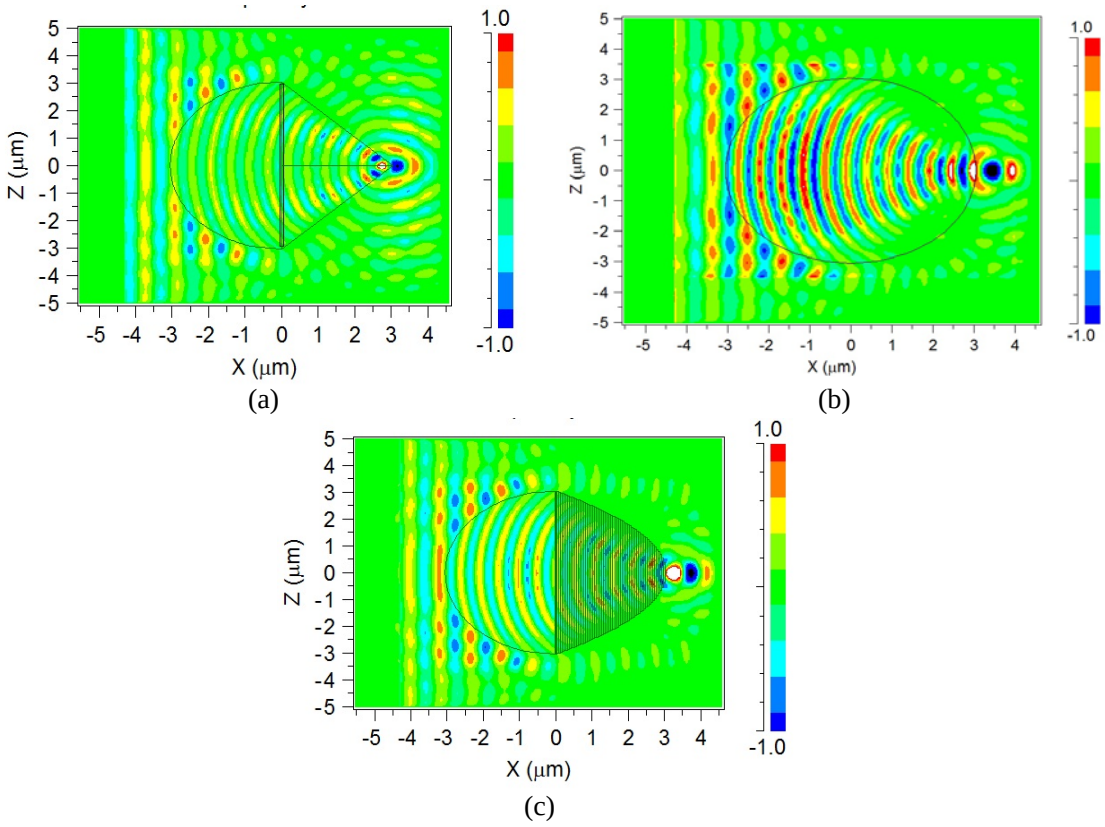

Figure 2. Electric field distribution in the x-z plane at 850 nm for (a) hybrid linear, (b) cylindrical, and (c) hybrid parabolic collimators on top of a silver metallic layer.

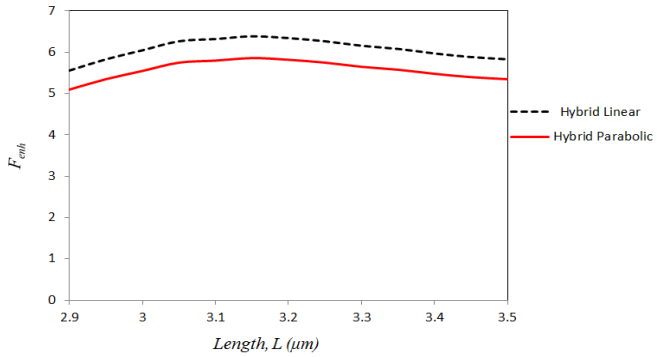

Figure 3. Electric field enhancement factor (F_{enh}) as a function of the length, L for hybrid linear (black dashed curve) and hybrid parabolic (red solid curve). The dielectric concentrators are placed on top of silver.

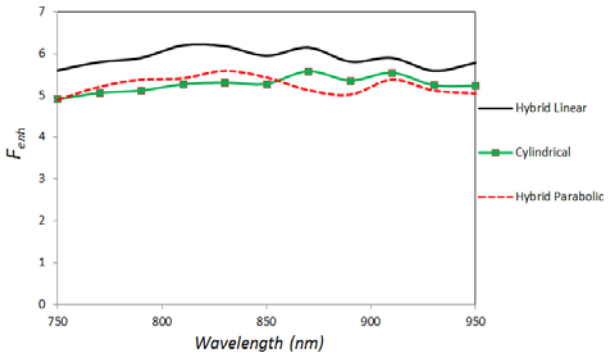

Figure 4. Electric field enhancement factor (F_{enh}) as a function of the wavelength for cylindrical (green solid curve with square markers), hybrid linear (black solid curve) and hybrid parabolic (red dashed curve). The dielectric concentrators are placed on top of silver.

when compared with the cylindrical shape. The spot size diameters at the exit of the structures are approximately 670 nm, 350 nm and 560 nm for the cylindrical, hybrid linear and hybrid parabolic shapes, respectively.

A more dramatic change occurs when the metal is changed from gold to either silver or aluminium. The electric field enhancement, when silver is used, increases by 10% to 20% when compared with gold

and can be attributed to the lower losses in silver [39] — however, silver can easily oxidize when exposed to air. The poor performance of aluminium is explained by its higher losses at 850 nm — its absorption coefficient is significantly higher than gold and silver. If silver and a hybrid linear structure are used, an overall improvement of 40% in F_{enh} over a cylindrical gold structure is achieved.

The effect of changing the length (L) on the electric field enhancement factor (F_{enh}) is shown in Figure 3: in both hybrid linear and parabolic, the electric field enhancement factors reach a maximum in the region between 3.0 µm and 3.15 µm (maximum values of 6.2 and 5.4 for the hybrid linear and parabolic structures, respectively). It might be expected that, at larger values of L, F_{enh} would be larger but that is not the case: as light propagates through the taper, there is always some amount of light being radiated — very long tapers may lose too much power through radiation before light reaches the end of the taper.

Figure 4 shows the electric field enhancement factor (F_{enh}) as a function of the wavelength for cylindrical (green solid curve with square markers), hybrid linear (black solid curve) and hybrid parabolic (red dashed curve) dielectric concentrators such a way that the dielectric concentrators are placed on top of silver. Since the production of nanojets is a result of multiple scattering inside the dielectric concentrator, it would be expected that the electric field enhancement factor (F_{enh}) to be dependent upon the wavelength: this can be observed in the oscillations in the curves for silver (Figure 4). F_{enh} reaches maxima at 830 nm and 870 nm what can be partially attributed to the higher plasma frequency of silver. The electric field enhancement factors (F_{enh}) at $\lambda = 850$ nm are 5.95, 5.28 and 5.43 for hybrid linear, cylindrical and hybrid parabolic structures, respectively. The maximum values found in Table 1 for silver do not occur at $\lambda = 850$ nm, as can be observed in Figure 4. The hybrid linear (black solid curve) provides higher enhancement than hybrid parabolic and cylindrical dielectric concentrators because of the smaller field diameter at the edge (lightning rod effect) of the hybrid linear dielectric concentrator.

It is true that a linear taper with a sharp edge cannot be fabricated in practice; thereby we studied the effect of a finite width at the end of the linear taper. Figures 5(a) and (b) show the electric field profile in the x-z plane at 850 nm for hybrid linear structure with the linear taper of 50 nm and 100 nm, respectively. For a finite width of the linear taper changing from 0 nm to 100 nm and, for the same linear taper length, F_{enh} changes from 6.2 to 6.5 — meaning that actually a taper not ending into a sharp edge can provide a larger electric field enhancement. Tens of nanometers features can be fabricated by using electron beam lithography and reactive ion etching systems.

In summary, plasmonic nanojets are studied for three different types of dielectric concentrators: cylindrical, hybrid linear and hybrid parabolic. The hybrid linear produces the highest electric field enhancement factor (edge effect) but at the expense of a divergent exit beam. The effects of different metals on the performance of nanojets: the lower are the metal losses, the higher is the electric field enhancement factor — thereby it is fair to say that silver works significantly better than aluminium in this type of application.

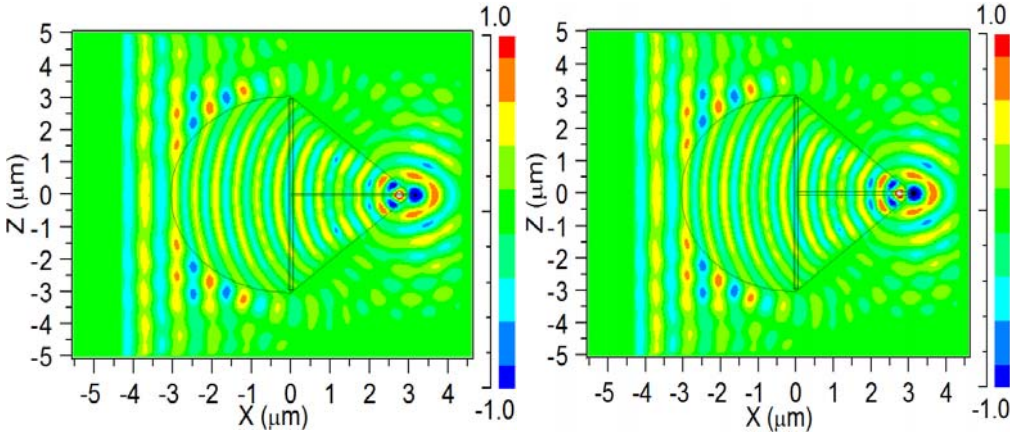

Figure 5. Electric field distribution in the x-z plane at 850 nm for hybrid linear collimator on top of a silver metallic layer with linear taper of (a) 50 nm and (b) 100 nm.

4. CONCLUSIONS

In this article, it is shown that a hybrid linear geometry can improve the electric field enhancement of plasmonic nanojets and, in addition to that, the losses in the metal play a major role in the performance of the device — in this aspect, silver works better than gold and aluminium because of its lower losses. Finally, an overall improvement of 40% in electric field enhancement factor (F_{enh}) over a cylindrical gold structure is achieved by using silver and a hybrid linear structure.

REFERENCES

1. Choi, S. J., K. Djordjev, and J. Dapkus, "Microdisk lasers vertically coupled to output waveguides," *IEEE Phot. Technol. Lett.*, Vol. 15, 1330–1332, 2003.
2. Fujita, M., A. Sakai, and T. Baba, "Ultra-small and ultra-low threshold microdisk laser — Design, fabrication, lasing characteristics and spontaneous emission factor," *IEEE J. Sel. Top. Quantum Electron.*, Vol. 5, 673–681, 1999.
3. Seassal, C., C. Monat, J. Mouette, E. Touraille, B. Ben Bhakir, H. T. Hattori, J. L. Leclercq, X. Letartre, P. Rojo-Romeo, and P. Viktorovitch, "InP bonded membrane photonic components and circuits: Towards 2.5 dimensional micro-nano-photonics," *IEEE J. Sel. Top. in Quantum Electron.*, Vol. 11, 395–407, 2005.
4. Levi, A. F. J., R. E. Slusher, S. L. McCall, J. L. Glass, S. J. Pearton, and R. A. Logan, "Directional light coupling from microdisk lasers," *Appl. Phys. Lett.*, Vol. 62, 561–563, 1993.
5. Park, H. G., J. K. Hwang, J. Huh, H. Y. Ryu, S. H. Kim, and Y. H. Lee, "Characteristics of modified single-defect two-dimensional photonic crystal lasers," *IEEE J. Quantum Electron.*, Vol. 38, 1353–1365, 2002.
6. Loncar, M. and A. Scherer, "Photonic crystal laser sources for chemical detection," *Appl. Phys. Lett.*, Vol. 82, 4648–4650, 2003.
7. Hattori, H. T., I. McKerracher, H. H. Tan, C. Jagadish, and R. M. De La Rue, "In-plane coupling of light from InP based photonic crystal band-edge lasers into single-mode waveguides," *IEEE J. Quantum Electron.*, Vol. 43, 279–286, 2007.
8. Yokohama, M. and S. Noda, "Finite-difference time-domain simulation of two-dimensional photonic crystal surface emitting laser," *Opt. Express*, Vol. 13, 2869–2880, 2005.
9. Hattori, H. T., X. Letartre, C. Seassal, P. Rojo-Romeo, J. L. Leclercq, and P. Viktorovitch, "Analysis of hybrid photonic crystal vertical cavity surface emitting lasers," *Opt. Express*, Vol. 11, 1799–1808, 2003.
10. Hill, M. T., M. Marell, E. S. P. Leong, B. Smallbrugge, Y. Zhu, M. Sun, P. J. Van Veldhoven, E. J. Geluk, F. Karouta, Y. S. Oei, R. Notzel, C. Z. Ning, and M. K. Smit, "Lasing in metal-insulator-metal sub-wavelength plasmonic waveguides," *Opt. Express*, Vol. 17, 11107–11112, 2009.
11. Stockman, M. I., "Spaser action, loss compensation and stability in plasmonic systems with gain," *Phys. Rev. Lett.*, Vol. 106, 156802, 2011.
12. Cubukcu, E., N. Yu, E. J. Smythe, L. Diehl, K. B. Crozier, and F. Capasso, "Plasmonic laser antennas and related devices," *IEEE J. Sel. Top. in Quantum Electron.*, Vol. 14, 1448–1461, 2008.
13. Hattori, H. T., Z. Li, D. Liu, I. D. Rukhlenko, and M. Premaratne, "Coupling of light from microdisk lasers into plasmonic nano-antennas," *Opt. Express*, Vol. 17, 20878–20884, 2009.
14. Ball, G. A., and W. M. Morey, "Continuously tunable single-mode erbium fiber laser," *Opt. Letters*, Vol. 19, 1979–1981, 1994.
15. Zyskind, J. L., V. Mizrahi, D. J. Di Giovanni, and J. W. SUlhoff, "Short single frequency erbium-doped fibre laser," *Electron. Lett.*, Vol. 28, 1385–1387, 1992.
16. Agrawal, G. P. and S. Radic, "Phase-shifted fiber Bragg grating and their applications for wavelength demultiplexing," *IEEE Phot., Technol. Lett.*, Vol. 6, 995–997, 1994.
17. Cazo, R. M., O. Lisboa, H. T. Hattori, V. M. Schneider, C. L. Barbosa, R. C. Rabelo, and J. L. S. Ferreira, "Experimental analysis of reflected modes in a multimode strained grating," *Microw. and Opt. Technol. Lett.*, Vol. 28, 4–8, 2001.

18. Oullette, F., "All-fiber filter for efficient dispersion compensation," *Opt. Letters*, Vol. 16, 303–305, 1991.
19. Hattori, H. T., V. M. Schneider, and O. Lisboa, "Cantor set fiber Bragg grating," *J. of Opt. Soc. America A*, Vol. 17, 1583–1589, 2000.
20. Barcelos, S., M. N. Zervas, and R. I. Laming, "Characteristics of chirped fiber gratings for dispersion compensation," *Opt. Fiber Technol.*, Vol. 1, 213–215, 1996.
21. Archambault, J. L., P. S. Russell, S. Barcelos, P. Hua, and L. Reekie, "Grating frustrated coupler: A novel channel-dropping filter in single-mode optical fiber," *Opt. Letters*, Vol. 19, 180–182, 1994.
22. Tailaert, D., W. Bogaerts, P. Bienstman, T. F. Krausss, P. Van Daele, I. Moerman, S. Verstuyft, K. De Mesel, and R. Baets, "An out-of-plane grating coupler for efficient butt-coupling between compact planar waveguides and single-mode fibers," *IEEE J. Quantum Electron.*, Vol. 38, 949–955, 2002.
23. Heifetz, A., S. C. Kong, A. V. Sahakian, A. Taflove, and V. Backman, "Photonic nanojets," *J. Comput. Theor. Nanosci.*, Vol. 6, 1979–1992, 2009.
24. Ferrand, P., J. Wenger, A. Devilez, M. Pianta, B. Stout, N. Bonod, E. Popov, and H. Rigneault, "Direct imaging of photonic nanojets," *Opt. Express*, Vol. 16, 6930–6940, 2008.
25. Heifetz, A., K. Huang, A. V. Sahakian, X. Li, A. Taflove, and V. Backman, "Experimental confirmation of backscattering enhancement induced by a photonic jet," *Appl. Phys. Lett.*, Vol. 89, 221118, 2006.
26. Fletcher, D. A., K. E. Goodson, and G. S. Kino, "Focusing in microlenses close to a wavelength in diameter," *Opt. Letters*, Vol. 26, 399–401, 2001.
27. Chen, Z., A. Taflove, and V. Backman, "Photonic nanojet enhancement of backscattering of light by nanoparticles: A potential novel visible-light ultramicroscopy technique," *Opt. Express*, Vol. 12, 1214–1220, 2004.
28. Li, X., Z. Chen, A. Taflove, and V. Backman, "Optical analysis of nanoparticles via enhanced backscattering facilitated by 3-D photonic nanojets," *Opt. Express*, Vol. 13, 526–533, 2005.
29. Kim, M. S., T. Scharf, S. Mühlig, C. Rockstuhl, and H. P. Herzig, "Engineering photonic nanojets," *Opt. Express*, Vol. 19, 10206–10220, 2011.
30. Yi, K. J., H. Wang, Y. F. Lu, and Z. Y. Yang, "Enhanced Raman scattering by self-assembled silica spherical microparticles," *J. of Appl. Phys.*, Vol. 101, 063528, 2007.
31. Le Ru, E. C., E. Blackie, M. Meyer, and P. G. Etchegoin, "Surface enhanced Raman scattering enhancement factors: A comprehensive study," *J. Phys. Chem. C*, Vol. 111, 13794–13803, 2007.
32. Banaee, M. G. and K. B. Crozier, "Gold nanorings as substrate for surface-enhanced Raman scattering," *Opt. Letters*, Vol. 35, 760–762, 2010.
33. Li, Z., H. T. Hattori, P. Parkinson, J. Tian, L. Fu, H. H. Tan, and C. Jagadish, "A plasmonic staircase nano-antenna device with strong electric field enhancement for surface enhanced Raman scattering (SERS) applications," *J. Phys. D: Appl. Phys.*, Vol. 45, 305102, 2012.
34. Ashok, P. C., G. P. Singh, K. M. Tan, and K. Dholakia, "Fiber probe based microfluidic raman spectroscopy," *Opt. Express*, Vol. 18, 7642–7649, 2010.
35. Ju, D., H. Pei, Y. Jiang, and X. Sun, "Controllable and enhanced nanojet effects excited by surface plasmon polariton," *Appl. Phys. Lett.*, Vol. 102, 171109, 2013.
36. Fullwave 6.0 RSOFT Design Group, 1999.
37. Udagedara, I., M. Premaratne, I. D. Rukhlenko, H. T. Hattori, and G. P. Agrawal, "Unified PML for FDTD modelling of dispersive optical materials," *Opt. Express*, Vol. 17, 21179–21190, 2009.
38. Maier, S. A., *Plasmonics: Fundamentals and Applications,* New York, Springer, 2007.
39. Rakic, A. D., A. B. Djurisic, J. M. Elazar, and M. L. Majewski, "Optical properties of metallic films for vertical-cavity optoelectronic devices," *Appl. Optics*, Vol. 37, 5271–5283, 1998.